Journal of Alloys and Compounds 596 (2014) 58–62

Contents lists available at ScienceDirect

Journal of Alloys and Compounds

journal homepage: www.elsevier.com/locate/jalcom

Magnetic and magnetocaloric properties of equiatomic alloys *R*Al (*R* = Ho and Er)

L.H. Yang [a,b], H. Zhang [c], F.X. Hu [b], J.R. Sun [b], L.Q. Pan [a], B.G. Shen [b,*]

[a] Department of Physics, University of Science and Technology Beijing, Beijing, 100083, PR China
[b] State Key Laboratory for Magnetism, Institute of Physics, Chinese Academy of Sciences, Beijing 100190, PR China
[c] School of Materials Science and Engineering, University of Science and Technology Beijing, Beijing 100083, PR China

ARTICLE INFO

Article history:
Received 26 September 2013
Received in revised form 27 January 2014
Accepted 27 January 2014
Available online 4 February 2014

Keywords:
DyAl-type structure
Magnetocaloric effect
Metamagnetic transition

ABSTRACT

Magnetic and magnetocaloric properties of binary equiatomic alloys *R*Al (*R* = Ho and Er) are investigated in this work. HoAl compound undergoes antiferromagnetic (AFM)–ferromagnetic (FM) transition at T_1 = 13 K, and FM-paramagnetic (PM) transition at the Curie temperature T_C = 20 K, with temperature increasing. ErAl compound exhibits AFM-PM transition at the Néel temperature T_N = 9 K. The maximal values of magnetic entropy change (ΔS_M) are −22.5 J kg^{-1} K^{-1} for HoAl and −16.4 J kg^{-1} K^{-1} for ErAl for a magnetic field change of 0–5 T. The values of refrigerant capacity (RC) are 379.5 J kg^{-1} and 259.7 J kg^{-1} for HoAl and ErAl respectively. The large magnetocaloric effect makes *R*Al (*R* = Ho and Er) compounds promising candidates for low-temperature magnetic refrigerants.

1. Introduction

The magnetocaloric effect (MCE) is the thermal response of a magnetic material when subjected to magnetic field variation owing to the magneto-thermal coupling. It is characterized by the adiabatic temperature change ΔT_{ad} and the isothermal entropy change ΔS_M [1,2]. Based on this effect, magnetic refrigeration is one of the promising technologies, for its energy saving and environmental friendliness compared with the conventional vapor-compression technology, and consequently attracts lots of attention [1,3–5]. For practical application, intense investigations have been dedicated to room-temperature magnetic cooling materials, such as $Gd_5Si_2Ge_2$ [1,3], $La(Fe,Si)_{13}$ [6–8], MnAs [9–11], $MnFeP_{1-x}As_x$ [5,12,13], and Heusler alloys [14–16]. These materials undergo a first-order phase transition and exhibit giant magnetocaloric effect. At the same time, materials for low-temperature magnetic refrigeration also attracts a great deal of interest for the potential application in the refrigeration of gas (nitrogen, hydrogen, and helium) liquefaction, such as *R*FeSi (*R* = Tb, Dy [17], and Er [18]), some Tm based intermetallic compounds (TmGa [19], TmCuAl [20], and Tm_3Co [21]), and $ErMn_2Si_2$ [22].

Except materials mentioned above, we search and develop new magnetocaloric materials and pay attention to rare-earth based intermetallic compounds for large atomic moments of rare-earth elements. There are few articles on binary equiatomic alloys *R*Al (*R* = Gd, Tb, Dy, Ho, and Er), especially on magnetocaloric effect of them [23–27]. The *R*Al compounds crystallize in the DyAl-type orthorhombic structure with *Pbcm* space group. It is formed from aluminum chains and trigonal prism similar to a half-cell of CsCl [28]. The *R*Al compounds are antiferromagnetic with T_N of 42 K, 72 K, 20 K, and 10 K for *R* = Gd, Tb, Dy, and Er, respectively. However, HoAl is ferromagnetic with T_C of 26 K [24,28]. In present work, we carried out a further study on the magnetic and magnetocaloric properties of *R*Al (*R* = Ho and Er) compounds.

2. Experimental details

*R*Al (*R* = Ho and Er) compounds were prepared by arc melting appropriate amounts of high-purity elements in argon atmosphere. The cast samples were sealed in an evacuated quartz tube and annealed at 1173 K for 30 days, then quenched in liquid nitrogen. The crystalline structures and the crystal lattice parameters of compounds were determined by the room-temperature X-ray powder diffraction and the Rietveld refinement. The isothermal and isofield magnetic properties were measured in a MPMS SQUID VSM magnetometer from Quantum Design Inc.

3. Results and discussion

Fig. 1 shows the room-temperature X-ray diffraction (XRD) patterns and Rietveld refinement of HoAl and ErAl compounds. The results indicate that both HoAl and ErAl crystallize in orthorhombic DyAl-type structure. The calculated lattice parameters are a = 5.8065 Å, b = 11.3357 Å, and c = 5.5852 Å for HoAl compound

* Corresponding author.
E-mail address: shenbg@aphy.iphy.ac.cn (B.G. Shen).

http://dx.doi.org/10.1016/j.jallcom.2014.01.202
0925-8388/

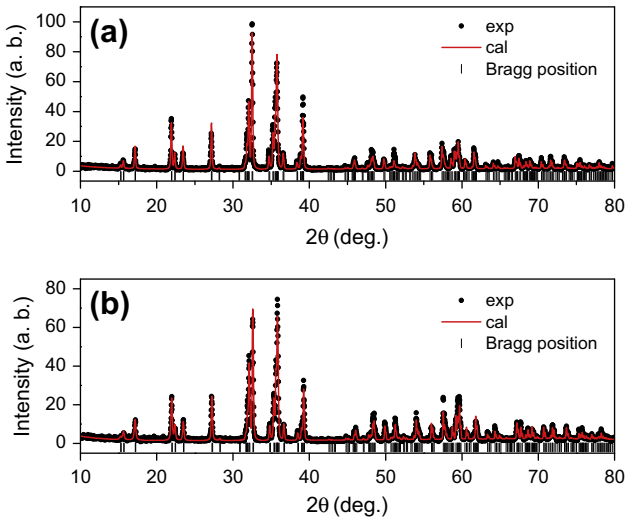

Fig. 1. Room-temperature XRD and Rietveld refinement of *R*Al (*R* = Ho and Er) compounds.

and $a = 5.7832$ Å, $b = 11.2799$ Å, and $c = 5.5644$ Å for ErAl compound, respectively. These values are consistent with the values reported before [26,27].

Fig. 2(a) and (b) displays the zero-field-cooling magnetization curves (M–T) of HoAl and ErAl under a field of 0.01 T, respectively. From Fig. 2(a), it is observed that HoAl compound undergoes two successive transitions at 13 K and 20 K respectively. This result is consistent with the previous report. Bécle et al. [28] reported that HoAl was ferromagnetic under $T_C = 26$ K. Meanwhile, he pointed out that the neutron diffraction pattern at 4.2 K exhibited the characteristic of the coexistence of an antiferromagnetic and ferromagnetic arrangement. Consequently, the observed two phase transitions could be corresponding to AFM–FM transition at $T_1 = 13$ K and FM–PM transition at $T_C = 20$ K, respectively. This analysis can be confirmed by the isothermal magnetization curves and magnetic field dependence of magnetic entropy change. Fig. 2(b) presents the M–T curve of ErAl compound. A typical magnetic transition from AFM to PM at $T_N = 9$ K is observed. This result is in agreement with the result reported before. The insets of Fig. 2(a) and (b) show the Curie–Weiss fits of HoAl and ErAl in the PM region, respectively. The effective paramagnetic moments per R atom (R = Ho and Er) are $11.0\mu_B$ and $9.8\mu_B$, close to the free ion values ($10.6\mu_B$ for Ho^{3+} and $9.6\mu_B$ for Er^{3+}).

The isothermal magnetization curves (M–H) of HoAl and ErAl are measured under applied fields up to 5 T in a vide temperature range. Fig. 3(a) shows the M–H curve of HoAl compound. There is not obvious magnetic hysteresis, which is important for practical application of magnetic refrigerant materials. Fig. 3(b) presents the M–H curves in a temperature range from 5 to 15 K at low magnetic fields. The intersections among these curves are observed, which are caused by field-induced metamagnetic transition from AFM to FM state. The observed metamagnetic transition demonstrates the existence of antiferromagnetic state at low temperatures, which is in agreement with the result of M–T curve. Fig. 4(a) displays the M–H curves of ErAl compound. As an antiferromagnet, ErAl compound is expected to exhibit a metamagnetic transition below $T_N = 9$ K in the M–H curve. However, it is interesting that two successive field-induced transitions are observed in the temperature range of 5–9 K (shown in Fig. 4(b)). This result resembles the result of ErTiSi [29], in which a field-induced AFM–AFM transition and a subsequent AFM–FM metamagnetic transition were observed with increasing magnetic field at low temperatures. From Fig. 4(b), ErAl compound firstly undergoes a possible field-induced AFM-AFM transition at about 0.3 T and a succedent AFM–FM metamagnetic transition at about 1.2 T with increasing magnetic field at 5 K.

Associated with the rich transition behaviors, magnetic entropy changes ΔS_M are calculated by Maxwell's relation $\Delta S_M = \int_0^H \left(\frac{\partial M}{\partial T}\right) dH$. Fig. 5(a) displays the temperature dependence of $-\Delta S_M$ for different magnetic field changes for HoAl compound. The observed two peaks centered at about 8 K and 20 K are corresponding to the field-induced metamagnetic transition at T_1 and FM–PM transition at T_C, respectively. For a field change of 0–5 T, the maximal value of $-\Delta S_M$ for HoAl reaches 22.5 J kg^{-1} K^{-1} at 20 K. Fig. 5(b) presents the temperature dependence of $-\Delta S_M$ for ErAl compound. It is seen clearly that the value of $-\Delta S_M$ are negative at low temperatures under low fields. With increasing temperature and magnetic field,

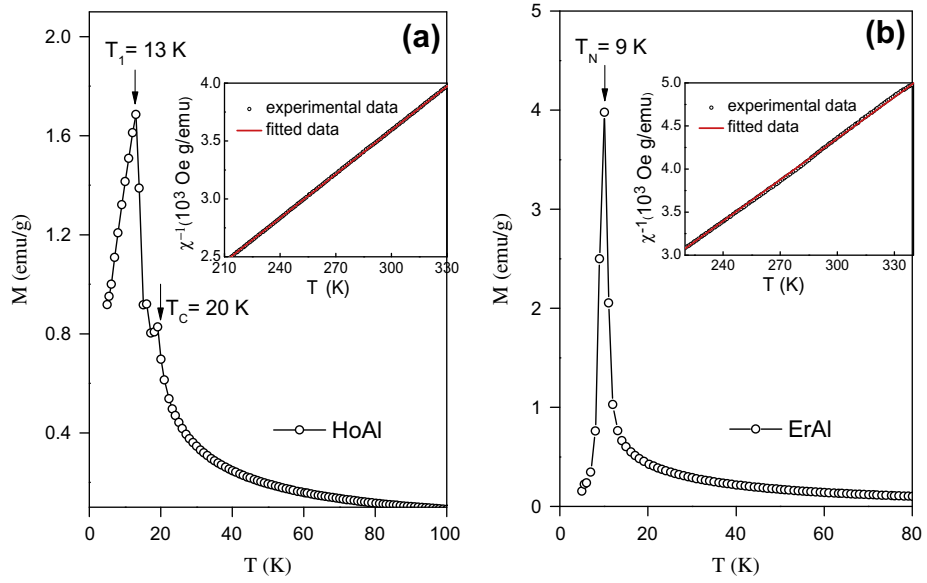

Fig. 2. Temperature dependences of zero-field-cooling magnetization for HoAl (a) and ErAl (b) under 0.01 T. The insets of (a) and (b) are the Curie–Weiss fits for HoAl and ErAl, respectively.

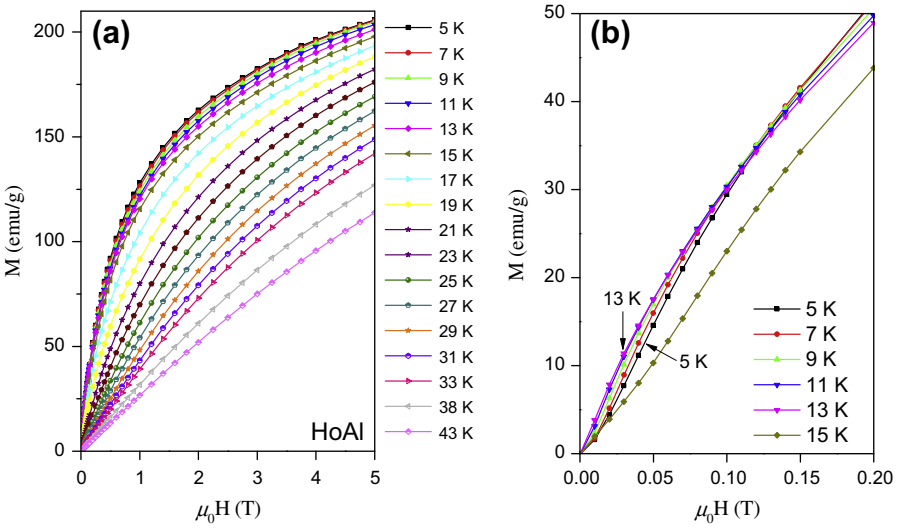

Fig. 3. (a) Isothermal magnetization curves (M–H) of HoAl in the temperature range of 5–43 K. (b) Isothermal magnetization curves in low magnetic field at 5 K, 7 K, 9 K, 11 K, 13 K, and 15 K.

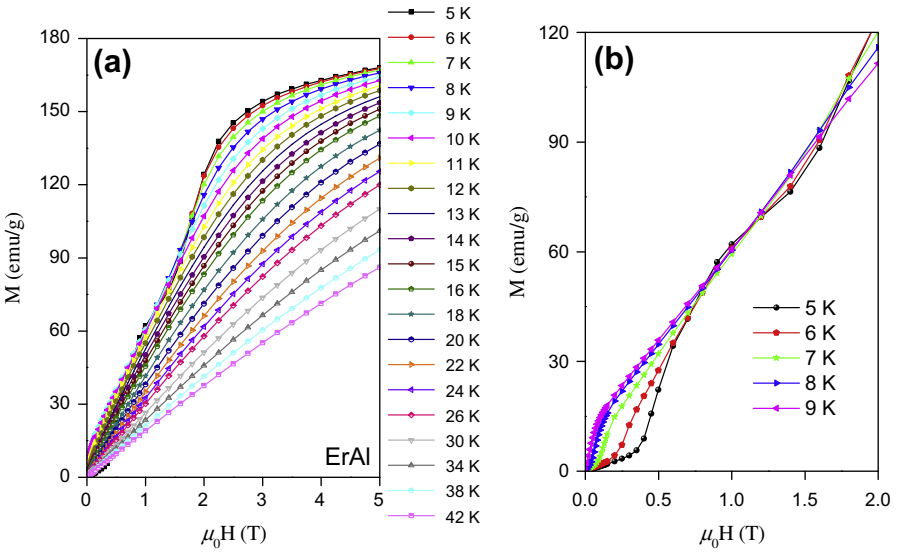

Fig. 4. (a) Magnetic isothermals of ErAl in the temperature range of 5–42 K. (b) Magnetic isothermals in low magnetic field at 5 K, 6 K, 7 K, 8 K, and 9 K.

the values change to be positive, due to field-induce AFM–FM transition. The peak of $-\Delta S_M$ for ErAl is about 16.4 J kg^{-1} K^{-1} at 12 K for a field change up to 5 T. The large MCE of HoAl and ErAl are comparable to those of some promising magnetic refrigerant materials working in low temperatures, such as DyNiAl (19 J kg^{-1} K^{-1}) [30], (Er,Gd)NiAl (10–22 J kg^{-1} K^{-1}) [31], $DyAl_2$ (19 J kg^{-1} K^{-1}) [32], $DyNi_2$ (22 J kg^{-1} K^{-1}) [32], and $TmAl_2$ (35.9 J kg^{-1} K^{-1} for ΔH = 7 T) [33].

The study on the magnetic field dependence of magnetic entropy change has been investigated intensively [34–36]. According to mean-field approximation, the magnetic entropy change can be expressed as $\Delta S_M \propto H^n$, where the exponent n is 2/3 at T_C. Fig. 6(a) presents mean-field approximation fit of HoAl at 20 K, indicating that n is 0.84. The value of n is close to the value of mean-field approximation and the minor deviation may be due to moderate applied fields. The inset of Fig. 6(a) shows the magnetic field dependence of $-\Delta S_M$ of HoAl at 6 K. Due to antiferromagnetic state of HoAl at 6 K, a change of sign in $-\Delta S_M$ is observed, which is consistent with the M–T and M–H analysis. Fig. 6(b) shows the magnetic field dependence of $-\Delta S_M$ of ErAl compound at 5.5 K. As ErAl is antiferromagnetic at 5.5 K, the change of sign in $-\Delta S_M$ is also observed.

Another important parameter to characterize the MCE is the refrigeration capacity (RC), which is related to the heat transferred between the cold and hot sinks during one ideal refrigeration cycle. The value of RC is calculated by integrating the area under the S_M $-T$ curve, using the temperatures at half-maximum of the peak as the integration limits. The RC values are obtained to be 379.5 J kg^{-1} and 259.7 J kg^{-1} for HoAl and ErAl, respectively.

4. Conclusions

In conclusion, we have studied the structural, magnetic and magnetocaloric properties of equiatomic compounds RAl (R = Ho and Er). Both HoAl and ErAl crystallize in orthorhombic DyAl-type structure. HoAl compound exhibits two successive magnetic transitions with increasing temperature, a AFM–FM transition at 13 K

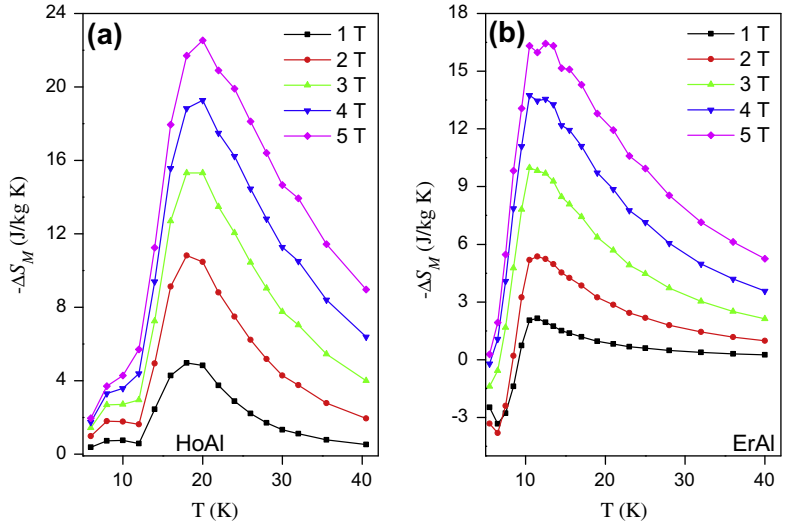

Fig. 5. Magnetic entropy change ΔS_M as a function of temperature of HoAl (a) and ErAl (b) for different magnetic field changes up to 5 T.

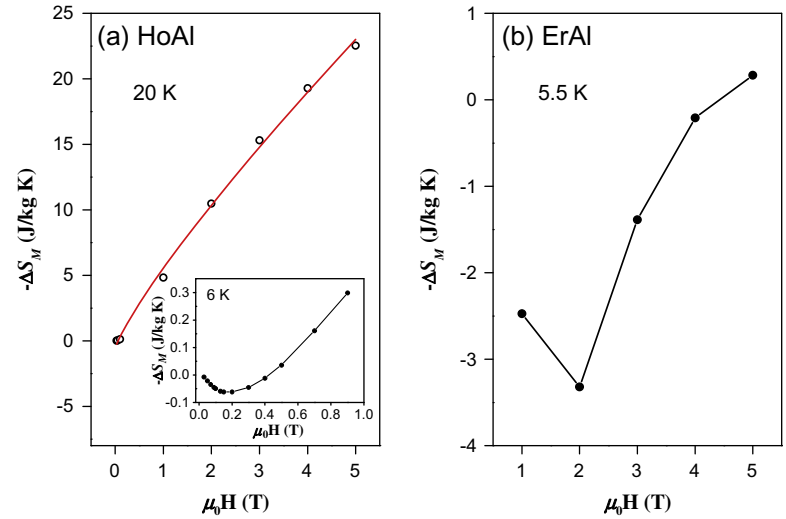

Fig. 6. Magnetic field dependence of magnetic entropy change of HoAl (a) at 20 K and ErAl (b) at 5.5 K. The inset of is the magnetic field dependence of $-\Delta S_M$ of HoAl at 6 K.

followed by a FM–PM transition at 20 K. ErAl compound undergoes a AFM–PM transition at 9 K. For a magnetic field change of 0–5 T, the values of $-\Delta S_M$ and RC of HoAl are found to be 22.5 J kg^{-1} K^{-1} and 379.5 J kg^{-1} respectively, while the corresponding values of ErAl are 16.4 J kg^{-1} K^{-1}and 259.7 J kg^{-1} respectively. The large MCE make *R*Al (*R* = Ho and Er) compounds promising candidates for cryogenic refrigeration.

Acknowledgements

This work was supported by the National Natural Science Foundation of China (Contract Nos. 11274357, 51001077), the Knowledge Innovation Project of the Chinese Academy of Sciences.

References

[1] K.A. Gschneidner Jr., V.K. Pecharsky, A.O. Tsokol, Rep. Prog. Phys. 68 (2005) 1479–1539.
[2] A.M. Tishin, J. Magn. Magn. Mater. 316 (2007) 351–357.
[3] V.K. Pecharsky, K.A. Gschneidner Jr., Phys. Rev. Lett. 78 (1997) 4494–4497.
[4] Z.B. Guo, Y.W. Du, J.S. Zhu, H. Huang, W.P. Ding, D. Feng, Phys. Rev. Lett. 78 (1997) 1142–1145.
[5] O. Tegus, E. Brück, K.H.J. Buschow, F.R. de Boer, Nature (London) 415 (10) (2002) 150–152.
[6] F.X. Hu, B.G. Shen, J.R. Sun, X.X. Zhang, Chin. Phys. 9 (2000) 550–553.
[7] F.X. Hu, B.G. Shen, J.R. Sun, Z.H. Chen, G.H. Rao, X.X. Zhang, Appl. Phys. Lett. 78 (2001) 3675–3677.
[8] B.G. Shen, J.R. Sun, F.X. Hu, H.W. Zhang, Z.H. Chen, Adv. Mater. 21 (2009) 4545–4564.
[9] H. Wada, Y. Tanabe, Appl. Phys. Lett. 79 (2001) 3302–3304.
[10] S. Gama, A.A. Coelho, A. de Campos, A.M.G. Carvalho, F.C.G. Gandra, Phys. Rev. Lett. 93 (2004) 2372021–2372024.
[11] A. de Campos, D.L. Rocco, et al., Nat. Mater. 5 (2006) 802–804.
[12] E. Brück, O. Tegus, X.W. Li, F.R. de Boer, K.H.J. Buschow, Physica B 327 (2003) 431–437.
[13] O. Tegus, E. Brück, X.W. Li, L. Zhang, W. Dagula, F.R. de Boer, K.H.J. Buschow, J. Magn. Magn. Mater. 272–276 (2004) 2389–2390.
[14] F.X. Hu, B.G. Shen, J.R. Sun, Appl. Phys. Lett. 76 (2000) 3460–3462.
[15] T. Krenke, E. Duman, M. Acet, E.F. Wassermann, X. Moya, L. Mañosa, A. Planes, Nat. Mater. 4 (2005) 450–454.
[16] J. Liu, T. Gottschall, K.P. Skokov, J.D. Moore, O. Gutfleisch, Nat. Mater. 11 (2012) 620–626.
[17] H. Zhang, Y.J. Sun, E. Niu, L.H. Yang, J. Shen, F.X. Hu, J.R. Sun, B.G. Shen, Appl. Phys. Lett. 103 (2013) 2024121–2024125.
[18] H. Zhang, B.G. Shen, Z.Y. Xu, J. Shen, F.X. Hu, J.R. Sun, Appl. Phys. Lett. 102 (2013) 0924011–0924014.
[19] Z.J. Mo, J. Shen, L.Q. Yan, C.C. Tang, J. Lin, J.F. Wu, J.R. Sun, L.C. Wang, X.Q. Zheng, B.G. Shen, Appl. Phys. Lett. 103 (2013) 0524091–0524094.
[20] Z.J. Mo, J. Shen, L.Q. Yan, J.F. Wu, L.C. Wang, J. Lin, C.C. Tang, B.G. Shen, Appl. Phys. Lett. 102 (2013) 1924071–1924074.

[21] Z.J. Mo, J. Shen, L.Q. Yan, J.F. Wu, C.C. Tang, B.G. Shen, J. Alloys Comp. 572 (2013) 1–4.
[22] L. Li, K. Nishimura, W.D. Hutchison, Z. Qian, D. Huo, T. Namiki, Appl. Phys. Lett. 100 (2012) 1524031–1524034.
[23] K.H.J. Buschow, J.H.N. van Vucht, Philips Res. Rep. 22 (1967) 233–245.
[24] J.K. Yakinthos, F. Tchéou, Solid State Commun. 18 (1976) 1287–1289.
[25] J.K. Yakinthos, E. Roudaut, D. Fruchart, J. Magn. Magn. Mater. 28 (1982) 51–54.
[26] C. Bècle, R. Lemaire, Acta Crystallogr. 23 (1967) 840–845.
[27] K.H.J. Buschow, J. Less-Common Met. 8 (1965) 209–212.
[28] C. Bécle, R. Lemaire, D. Paccard, J. Appl. Phys. 41 (1970) 855–863.
[29] J. Shen, J.L. Zhao, F.X. Hu, J.F. Wu, M.Q. Gong, Y.X. Li, J.R. Sun, B.G. Shen, J. Appl. Phys. 107 (2010). 09A931-1-3.
[30] N.K. Singh, K.G. Suresh, R. Nirmala, A.K. Nigam, S.K. Malik, J. Appl. Phys. 99 (2006). 08K904-1-3.
[31] B.J. Korte, V.K. Pecharsky, K.A. Gschneidner, J. Appl. Phys. 84 (1998) 5677–5685.
[32] P.J. von Ranke, V.K. Pecharsky, K.A. Gschneidner Jr., Phys. Rev. B 58 (1998) 12110–12116.
[33] M. Patra, S. Majumdar, S. Giri, Y. Xiao, T. Chatterji, J. Alloys Comp. 531 (2012) 55–58.
[34] M. Patra, S. Majumdar, S. Giri, G.N. Iles, T. Chatterji, J. Appl. Phys. 107 (2010) 0761011–0761013.
[35] V. Franco, J.S. Blázquez, A. Conde, Appl. Phys. Lett. 89 (2006) 2225121–2225123.
[36] Q.Y. Dong, H.W. Zhang, J.R. Sun, B.G. Shen, V. Franco, J. Appl. Phys. 103 (2008) 1161011–1161013.